Thin Solid Films 520 (2012) 5000–5006

Contents lists available at SciVerse ScienceDirect

Thin Solid Films

journal homepage: www.elsevier.com/locate/tsf

# Stable *p*-type conductivity and enhanced photoconductivity from nitrogen-doped annealed ZnO thin film

Soumen Dhara, P.K. Giri *

*Department of Physics, Indian Institute of Technology Guwahati, Guwahati-781039, India*

ARTICLE INFO

*Article history:*
Received 20 July 2011
Received in revised form 16 February 2012
Accepted 23 February 2012
Available online 3 March 2012

*Keywords:*
*p*-type ZnO
Photoconductivity
Sputtering
Nitrogen doping

ABSTRACT

We report on the growth of p-type ZnO thin films with improved stability on various substrates and study the photoconductive property of the p-type ZnO films. The nitrogen doped ZnO (N:ZnO) thin films were grown on Si, quartz and alumina substrates by radio frequency magnetron sputtering followed by thermal annealing. Structural studies show that the N:ZnO films possess high crystallinity with c-axis orientation. The as-grown films possess higher lattice constants compared to the undoped films. Besides the high crystallinity, the Raman spectra show clear evidence of nitrogen incorporation in the doped ZnO lattice. A strong UV photoluminescence emission at ~380 nm is observed from all the N:ZnO thin films. Prior to post-deposition annealing, *p*-type conductivity was found to be unstable at room temperature. Post-growth annealing of N:ZnO film on Si substrate shows a relatively stable p-type ZnO with room temperature resistivity of 0.2 Ω cm, Hall mobility of 58 $cm^2/V\,s$ and hole concentration of $1.95\times10^{17}\ cm^{-3}$. A homo-junction *p*–*n* diode fabricated on the annealed p-type ZnO layer showed rectification behavior in the current–voltage characteristics demonstrating the *p*-type conduction of the doped layer. Doped ZnO films (annealed) show more than two orders of magnitude enhancement in the photoconductivity as compared to that of the undoped film. The transient photoconductivity measurement with UV light illumination on the doped ZnO film shows a slow photoresponse with bi-exponential growth and bi-exponential decay behaviors. Mechanism of improved photoconductivity and slow photoresponse is discussed based on high mobility of carriers and photodesorption of oxygen molecules in the N:ZnO film, respectively.



## 1. Introduction

ZnO has attracted much attention as a promising material for the ultraviolet light emitting diodes and lasers because of its wide band gap of 3.37 eV, large excitation binding energy (60 meV) and high optical gain (320 $cm^{-1}$) at room temperature [1,2]. For the device fabrication, both *n*-type and *p*-type ZnO are essential. However, the as-grown ZnO film grown by different techniques usually show *n*-type behavior due to intrinsic defects. Moreover, high quality *n*-type ZnO can be obtained by doping with group III elements such as Ga, Al and In [3–5]. The major hurdle for the development of ZnO-based optoelectronic devices is the lack of good and reproducible *p*-type conduction [6]. And also it is observed that *p*-type conduction is very unstable even at room temperature and easily converts to *n*-type conduction during storage [7–9]. The *p*-type doping in ZnO is difficult due to various reasons, such as deep acceptor level, low solubility of acceptor dopant and native donor defects like zinc interstitial ($Zn_i$) and oxygen vacancy ($V_o$) [10–14]. Different sources, such as phosphorus, $N_2$, NO, $N_2O$, $NH_3$, arsenic had been used to prepare *p*-type ZnO by N doping [6,12,15–18]. However, the results are controversial, as some groups reported only *n*-type conductivity in N:ZnO [13], while a few other groups reported *p*-type conduction in N:ZnO [14,19,20]. Moreover, most of the *p*-type N:ZnO films have low carrier mobility and are not stable. For example, it was reported that *p*-type N:ZnO reverted to *n*-type N:ZnO in a period of several days after deposition [19]. Further, a few groups reported instability of *p*-type conduction in the dark and its gradual transformation to *n*-type. However, as the n-type N:ZnO was irradiated with sunlight for a few minutes, it reverted back to *p*-type in the dark as well as in the light [20]. There have been attempts to utilize co-doping process to enhance its stability. The *p*-type films grown by co-doping process using $N_2$ and tellurium show enhanced electrical and optical properties, but it fails to remain *p*-type for long time [21]. Interestingly, a recent theoretical study [22] concludes that nitrogen is a deep acceptor in ZnO and it cannot lead to the hole conductivity. However, it contradicts several experimental results and does not consider the possibility of defect complex formation that may give rise to p-type conductivity [23,24]. Through first-principles density-functional theory calculations, Duan et al. [23] shows that the valence band maximum characteristic of ZnO can be altered by compensated donor-acceptor pairs, thus improving the p-type dopability. Therefore, it is necessary to investigate the mechanism/origin of hole conductivity in the *p*-type ZnO films in order to achieve a stable and reproducible p-type doping. While there

* Corresponding author. Fax: +91 361 2582749.
*E-mail address:* giri@iitg.ernet.in (P.K. Giri).

0040-6090/$ – see front matter © 2012 Elsevier B.V. All rights reserved.
doi:10.1016/j.tsf.2012.02.081

have been extensive studies on the electrical conductivity of N:ZnO films, there are very few studies on the UV photoconductivity (PC) of *p*-type ZnO. Further, the reported conductivity values are often very low [21,25]. Hence, there is a growing need to understand the origin of enhanced PC in *p*-type ZnO films for the fabrication of photodetectors. Doped ZnO film with high photoconductive response is highly desirable for the design of efficient photodetectors.

In this work, we attempt to prepare a stable *p*-type ZnO film on Si(100), alumina and quartz substrates by nitrogen doping using radio frequency (RF) sputter deposition. The electrical conductivity of the film was measured by Hall effect, *p*–*n* junction formation and Seebeck voltage measurements and its stability was studied as a function of time and post-deposition annealing temperature. The structure, quality and optical properties of the undoped and doped ZnO films were characterized by various structural and optical tools. We further studied the photoconductive properties of the *p*-type N:ZnO films and discuss about the origin of enhanced PC and stability of the doped ZnO films.

## 2. Experimental details

The N:ZnO thin films were grown on three different substrates: Si(100), alumina and quartz using RF magnetron sputtering. An undoped ZnO target (99.999% purity, Kurt J. Lesker) was used as the ZnO source. For *p*-type doping, a mixture of high purity $N_2$ and Ar gas at a ratio of 1:4 was inserted during sputter deposition. Before the deposition, all the substrates were cleaned in trichloro-ethylene, acetone and methanol under ultrasonic bath for 15 min each and each time substrates were washed with de-ionized water. Finally, these were cleaned with dilute hydrofluoric acid to remove the native oxide layer followed by rinsing with de-ionized water and drying under nitrogen gas flow. Sputtering was carried out at a RF power of 120 W for 60 min at a chamber pressure of 0.8 Pa at room temperature. In this process, ~1 μm thick films were grown on the substrate. To compare the results of the N:ZnO films with the undoped one, undoped ZnO film was prepared under similar condition without $N_2$ gas flow during sputtering. Post deposition annealing was carried out at 500 °C for 1 h. To study about the reproducibility of the *p*-type conductivity, another set of three N:ZnO thin films were grown on Si, quartz and alumina substrates by keeping the same experimental conditions. The structure and morphology of the as-deposited and annealed films were studied by X-ray diffraction using Cu $K_\alpha$ X-ray radiation in 3° grazing angle (XRD, D8 Advance, Bruker), scanning electron microscopy (SEM, Leo 1430VP, Carl Zeiss) at 10 kV operating voltage with energy dispersive X-ray spectroscopy (EDX) and atomic force microscopy (AFM, Model 5500, Agilent Technologies) in the contact mode using a silicon nitride tip. Micro-Raman spectra of the films were measured in backscattering geometry using a 632 nm laser and a liquid nitrogen cooled charge coupled device detector (LabRAM HR-800, Jobin Yvon). The optical properties of the films were studied by photoluminescence (PL) (FS 920P, Edinburg) and UV–vis (3000pc, Shimadzu) spectrometer. The 325 nm laser excitation from a He–Cd laser was used for PL measurement at room temperature. Electrical properties were studied using standard four probe, Hall effect and Seebeck voltage measurement systems. The photocurrent and photoresponse were measured using a picoammeter (Keithley, Model 6487) under the illumination of a monochromated UV light (wavelength 360 nm) from a 150 W xenon lamp. The UV light is tightly focused onto the sample making sure that only the region between the two electrodes is fully illuminated.

## 3. Results and discussion

### 3.1. Structural studies

The structural characterization of the N:ZnO films was done by X-ray diffraction measurements, which are shown in Fig. 1. The XRD patterns show high crystallinity and c-axis orientation of hexagonal

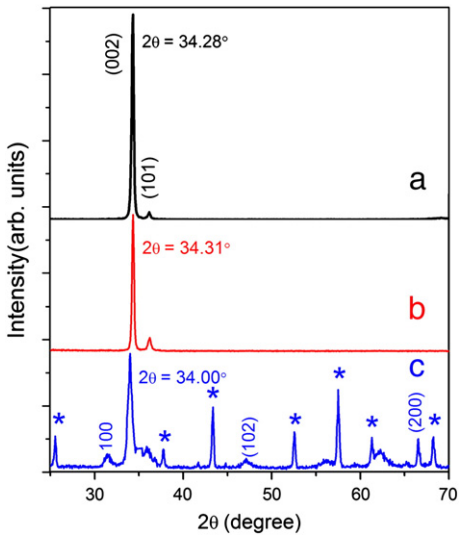


**Fig. 1.** XRD pattern of the N:ZnO thin films grown on: (a) Si, (b) quartz and (c) alumina substrates. The strong (002) peak indicates prefered c-axis orientation and high crystallinity of the doped ZnO films. The indicated 2θ value in each case corresponds to (002) peak position. The XRD peaks marked with asterisk (*) indicate contribution from alumina substrate.

ZnO phase. The N:ZnO films grown on Si and quartz substrates show better crystallinity compared to the film grown on the alumina substrate. The additional peaks (marked with *) in Fig. 1(c) are related to the XRD peaks of alumina substrate ($Al_2O_3$). No other phases (e.g. $Zn_3N_2$ or AlN) are detected in the XRD spectra, implying that nitrogen concentration in the N:ZnO films is below the solubility limit ruling out the possibility of $Zn_3N_2$ phase formation, as ZnO–$Zn_3N_2$ interface is the another source of *p*-type conductivity in the materials that are actually *n*-type [26]. The N:ZnO film grown on the alumina substrate does not show any preferential orientation due to larger lattice mismatch. The XRD peak positions (2θ values) of the N:ZnO films are found to be lower than that of the unstrained ZnO. The calculated lattice constants are $c = 5.223–5.269$ Å and $a = 3.260–3.288$ Å for the as-deposited N:ZnO films. These are larger than that of pure ZnO lattice ($c = 5.206$ Å and $a = 3.249$ Å) and the undoped ZnO film ($c = 5.218$ Å and $a = 3.256$ Å). The larger lattice constants can be attributed to internal tensile stress due to N atom incorporation in the ZnO lattice [27]. The average grain sizes of the N:ZnO films are calculated using Scherrer's equation [28]. The calculated grain sizes are 68, 67 and 12 nm for quartz, Si and alumina substrates, respectively. After post-growth annealing at 500 °C, the N:ZnO films show enhanced intensity of XRD peaks along with an increase in grain size, as expected. In the annealed films, the XRD peak moves (~0.08–0.23°) closer to the peak position of unstrained ZnO indicating a partial relaxation of strain. Therefore, after the annealing the structural quality of the N:ZnO films are enhanced and defects states are possibly reduced.

Since the PC of a semiconductor is usually controlled by surface effects [29], the surface morphologies of N:ZnO films were characterized by SEM and AFM analysis to understand the observed enhancement in PC. Fig. 2(a–c) show the surface morphology of the undoped, doped and annealed doped ZnO thin films grown on the Si substrate, respectively. It shows the formation of nanometer size grains in the films with varying sizes. The N:ZnO films show larger grain size compared to the undoped film. The measured grain size of the N:ZnO films varies from 112 to 500 nm. During annealing N:ZnO thin films recrystallized and forms a smooth surface with faint grain boundaries. Fig. 2(d–e) show the AFM surface topography images of the as-deposited and annealed N:ZnO films, respectively. The pebble like nanostructure formation is observed from all the films grown on different substrates. The measured root means square

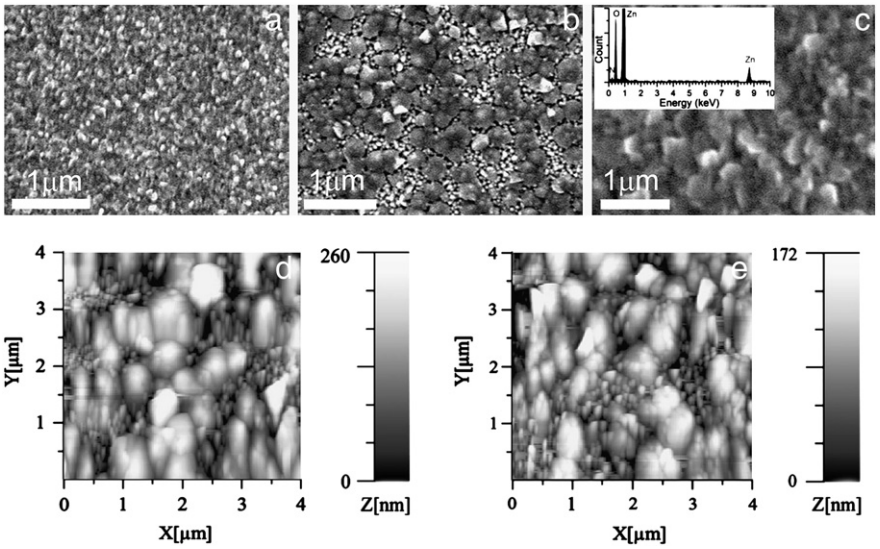


**Fig. 2.** The SEM images of the: (a) undoped, (b) N-doped and (c) annealed N-doped ZnO thin films grown on Si substrates. Inset of 2(c) shows the EDX data of the corresponding film. (d–e) AFM topography of the as-deposited and annealed doped films, respectively.

(*rms*) roughness is ~61.8 nm and ~40.5 nm for the as-deposited and annealed films grown on Si substrate. The reduction in *rms* roughness after annealing indicates the formation of smoother surface with better crystallinity of the film. The obtained smooth surface confirms the reduction in grain boundary in the annealed thin film. The nitrogen doping in the N:ZnO films are confirmed by EDX analysis. The EDX data of the annealed N:ZnO film grown on Si is shown in Fig. 2(c) as inset. According to normalized EDX elemental analysis, obtained elemental contents are Zn (49.8 at.%), O (48.8 at.%) and N(1.4 at.%). The EDX data of the N:ZnO films grown on quartz and alumina substrates show the presence of N. In general, it has been seen that the as-deposited undoped ZnO thin film is colorless while in this case the as-deposited N:ZnO films are yellow-orange colored, which further supports the incorporation of nitrogen atoms inside the ZnO lattice.

The nitrogen incorporation in the ZnO lattice and quality of the N:ZnO films were further studied by micro-Raman analysis. Fig. 3 shows the Raman spectra of the N:ZnO films grown on the Si and quartz substrates, respectively. The Raman spectra show characteristic Raman modes of hexagonal ZnO, indicating good crystallinity of the N:ZnO films. The Raman peaks at 438 $cm^{-1}$ and 580 $cm^{-1}$ correspond to $E_2^{high}$ and $A_1^{LO}$ modes of hexagonal ZnO, respectively. The additional Raman modes at 275, 510 and 643 $cm^{-1}$ correspond to the local vibrational modes of nitrogen [30]. Kaschner et al. [20] reported that the intensity of 275 $cm^{-1}$ mode strongly increases with the nitrogen concentration in N:ZnO films grown by chemical vapor deposition method. From the relative intensity of 275 $cm^{-1}$ band in N:ZnO film on quartz and Si substrates, it appears that nitrogen incorporation is higher in case of N:ZnO on quartz substrate. However, in case of Si substrate the nitrogen incorporation may be optimum for activation of dopants and this gives rise to enhanced electrical conductivity, as discussed later. Therefore, our Raman studies confirm nitrogen incorporation and presence Zn – N bond in the N:ZnO films. For comparison, the Raman spectrum of the undoped ZnO film is also shown in Fig. 3. The observed strong $E_2^{high}$ mode in undoped film indicates the presence of sufficient oxygen molecules in the ZnO, as the above mode is associated with the vibration of oxygen molecules. On the other hand, in N:ZnO films $A_1^{LO}$ mode is stronger than the $E_2^{high}$ mode, which indicates a high density of oxygen vacancy or zinc interstitials. It is likely that an interplay between these intrinsic defects and nitrogen related acceptors states have influence on the overall p-type behavior of the N:ZnO films.

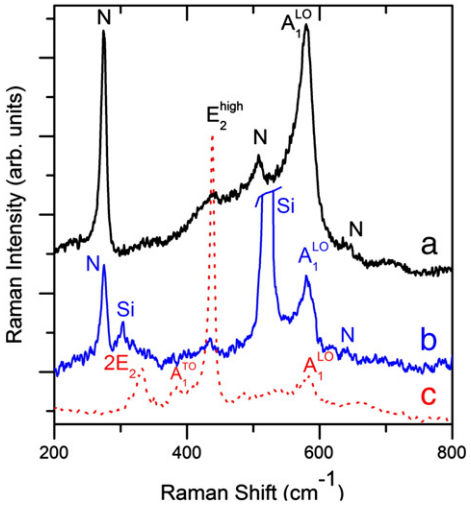


**Fig. 3.** Micro-Raman spectra of the *p*-type N:ZnO thin films grown on the (a) quartz and (b) Si substrate, respectively. (c) Micro-Raman spectrum of the undoped ZnO film.

### 3.2. Electrical characterization

For the electrical characterization, the N:ZnO films were cut into square shaped pieces. In the Hall measurement system, the tip of the four contacts were placed near the edge of each side of the square shaped N:ZnO film [31,32]. The Hall effect measurement of the as-deposited N:ZnO films show positive Hall coefficients (32–43 $cm^3$/C), which implies a *p*-type conduction in the as-deposited N:ZnO film. The electrical parameters of the as-deposited N:ZnO films calculated from four probe resistivity and Hall measurements are summarized in Table 1. The N:ZnO film grown on the Si substrate shows lowest electrical resistivity, highest carrier concentration and mobility of 0.2 Ω.cm, $1.95\times10^{17}$ $cm^{-3}$ and 58 $cm^2$/V.s, respectively. Our results

**Table 1**
Electrical parameters of the as-deposited N:ZnO films grown on different substrates.

| Substrate | Resistivity (Ω cm) | Hall mobility ($cm^2$/V s) | Carrier concentration ($cm^{-3}$) | Carrier type |
|---|---|---|---|---|
| Si | $0.202\pm0.003$ | $58\pm3.1$ | $1.95\times10^{17}$ | *p* |
| Quartz | $190.0\pm8.9$ | $0.22\pm0.010$ | $1.50\times10^{17}$ | *p* |
| Alumina | $200.0\pm12.3$ | $0.21\pm0.013$ | $1.45\times10^{17}$ | *p* |

are similar to the previous reports on *p*-type N:ZnO thin films grown by different methods [8,14,19,33]. However in the present case, the carrier mobility is relatively high compared to the previously reported values. Note that this mobility value is lower than that reported by Tsukazaki et al. [34] for the high quality single crystal N:ZnO epilayers grown on a lattice-matched substrate in ultra high vacuum. In case of N:ZnO films grown on the quartz and alumina substrates, relatively higher resistivity (~200 Ω.cm) and lower mobility (~0.2 $cm^2/V$) are obtained. This may be due to lower crystallinity of the N:ZnO films grown on alumina and quartz substrates. Details of the resistivity, Hall mobility, carrier concentration and carrier type of the as-deposited films are presented in Table 1. Here, we have used a simple approach to obtain nitrogen doping in the ZnO thin films. Although $N_2$ is usually an *n*-type dopant, we observed a *p*-type conductivity due to ionization of nitrogen molecules during sputtering. The ionized nitrogen atoms, which are present on the O sites in the ZnO lattice possibly act as a shallow acceptors resulting in *p*-type conduction. Although, achieving a stable *p*-type conductivity in N:ZnO film is very difficult, in our case Hall measurements were repeated several times on different samples that show the *p*-type behavior. Previously Ohgaki et al. [35] experimentally showed that non-uniform film and improper electrode position can yield wrong carrier type from Hall measurement. Latter, proper contact positions were found out by Bierwagen et al. [32] using finite-element analysis of the sample electrostatic potential distribution. They showed that if the contacts of a square-shaped sample are placed in the corners/edge, the measured carrier type will be correct even in the case of macroscopically inhomogeneous carrier concentrations and/or mobilities. Keeping this in mind, Hall measurements were performed by placing the tip of the four contacts on the edge of each side of the square shaped films. The Hall measurements were repeated over several times by interchanging the contact positions yielding identical results. To study the reproducibility of *p*-type conduction behavior, the next set of N:ZnO films which were grown later were characterized by four probe and Hall measurements. The obtained Hall coefficients are positive (30–38 $cm^3/C$), which indicates the *p*-type conduction behavior of the second set films. Therefore, we are getting reproducible *p*-type conduction behavior from the nitrogen doped ZnO thin films.

To further confirm the *p*-type conductivity of the as-deposited films, Seebeck voltage measurement was carried out by generating a temperature gradient between two needle probes, one at room temperature and other at higher temperature. The thermo voltage was measured by making pressure contact with the needle probe on the sample. Here *p*-type hot end was connected to the positive terminal and cold end was connected to the negative terminal of the voltmeter. This measurement was repeated by placing the probe on different positions on the film and an average value is taken. The Seebeck voltage measurement shows negative thermo voltage. The negative sign of thermo voltage confirmed the *p*-type conductivity of the as-deposited films on different substrates [36].

In order to understand the room temperature stability of *p*-type conduction, electrical measurements on all the three samples were performed again after 30 days. Interestingly, it is found that all the N:ZnO films were reverted back to weak *n*-type conductivity. This type of instability in the *p*-type N:ZnO film has been reported earlier [19,20] and is explained on the basis of relaxation of lattice constants and hydrogen generated donors in the films. Either water moisture or other ambient impurities could supply hydrogen and thus be responsible for the observed alteration of the conductivity type. In order to achieve a more stable *p*-type conductivity, the *n*-type N:ZnO films were annealed at 500 °C for one hour in air ambient. Interestingly, all the annealed N:ZnO thin films show strong *p*-type conductivity, as seen from Seebeck voltage measurement. The *p*-type conductivity of the annealed films is retained even after sixteenth months, though the measured Seebeck voltage is reduced to half of the voltage measured earlier. It is reported that present of interfacial defects may be responsible for the apparent *p*-type conductivity in the N:ZnO films [10]. It is also considered that the hydrogen or any other impurities diffusion leads to an increase in donor density resulting a compensation of acceptors in the N:ZnO films. As the as-deposited N:ZnO films contain interface defects and high density of grain boundaries, which possibly increases the diffusion of impurities along the grain boundaries and interface defects. As a result, the *p*-type conductivity degrades with time and we obtained *n*-type conductivity after 30 days. During annealing, moisture or other ambient impurities are evaporated and hydrogen generated donors are removed from the film. Due to removal of the donors, *p*-type conductivity with improved stability is obtained. The characterizations of the annealed films show improvement in the morphology, structural quality and reduction in interface defects. Due to the reduction in interface defects and grain boundaries, the annealed film opposed the re-adsorption and diffusion of hydrogen or any other impurities to a better extent than the as-deposited film and maintained the *p*-type conductivity for prolonged duration. Note that the time scale for change in conductivity is very large here compared to the earlier reports. However, prolonged exposure to moisture can degrade the conductivity of the film and storage in vacuum chamber is essential to retain the *p*-type conductivity of these films. We have found that in the annealed film, the *p*-type conductivity is retained even after 20 months, as demonstrated by the fabrication of a homo-junction *p*–*n* diode on the p-ZnO film. Note that the present results show only an improved stability of p-type conduction in doped ZnO film, though it is not highly stable. We believe that nitrogen doping induces point defects in the ZnO crystal lattice and these defects along with possible trace impurities in the ZnO form defect complexes that effectively gives rise to p-type conductivity. For example, it has been reported that donor-acceptor pair can compensate the donor in ZnO and improve the p-type dopability in N-doped ZnO [23]. The lack of very long term stability in these films strongly hints the involvement of defect complexes in the observed p-type conductivity. Since the Si substrate used was n-type doped, possibility of p-type conductivity arising from substrate is ruled out. Further, if the substrate has any contribution to the observed p-type conductivity in doped ZnO, the type conversion observed in as-deposited film cannot be justified. Similarly, change of Sebeck voltage in annealed film after 20 months strongly points to the fact that the observed conductivity is intrinsic to the doped film, rather than the substrate.

Finally, to check the device performance of the annealed *p*-type ZnO layer, a homo-junction *p*–*n* diode was fabricated by depositing a thin *n*-type ZnO layer on the annealed *p*-type layer. The *n*-type ZnO layer was grown by sputter deposition in Ar atmosphere, without the use of nitrogen gas during the growth. The electrical contact was made by depositing silver paste on both the layers (diameter of the contact area ~1 mm) and one additional contact on the *p*-type layer and subsequent heat treatment at 500 °C for 10 min. Inset of Fig. 4 shows the schematic of the device structure and the corresponding current–voltage (I–V) characteristic of the *p*-type layer only. The I–V characteristic of the *p*-type layer shows nearly linear current–voltage characteristic, which indicates the formation of good Ohmic contacts after the heat treatment at 500 °C for 10 min. The I–V characteristic of the homo-junction diode is shown in Fig. 4 that demonstrates a typical rectification behavior of the junction diode with a threshold voltage 2.0 V. This rectification behavior confirms the *p*-type conductivity of the N:ZnO layer. Similar I–V characteristics of homo-junction diode have also been reported by several groups using *p*-type N:ZnO layer [34,37]. Thus, the *p*–*n* junction characteristic clearly demonstrates that the annealed N:ZnO films are indeed p-type without experimental artifacts.

### 3.3. Optical absorption and PL studies

In order to study the optical absorption characteristics of the N:ZnO films, UV–vis absorption measurements were carried out for

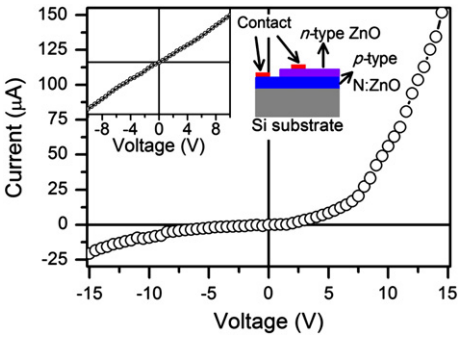


**Fig. 4.** Current–voltage (I–V) characteristic of the ZnO based homo-junction *p*–*n* diode made on the annealed N:ZnO film. Insets show the schematic of the fabricated device and I–V curve of the p-type layer only by making one additional contact on the N:ZnO film.

as-deposited and annealed films. Fig. 5(a) shows the optical absorption spectra of the N:ZnO film grown on the quartz substrate, which show a sharp peak at 368 nm. Fig. 5(b) shows the transmittance of the above film which lies in the range 61–64% for the wavelength region of 400–800 nm. This indicates a high optical transparency of the doped film in the visible region, which is of crucial importance for optoelectronic applications. The band gap of the N:ZnO film is calculated from the linear fit to the linear portion of the $(\alpha h\nu)^2$ vs. $h\nu$ plot, and is shown in Fig. 5(c). The calculated band gap is 3.24 eV, which is smaller than the band gap of the pure undoped ZnO (3.37 eV). This band gap narrowing is due to the incorporation of the N atoms inside the ZnO lattice [33]. The annealed N:ZnO film shows a slight increase in band gap with a band gap of 3.26 eV due to the recrystallization and relaxation of tensile stress. Our results are consistent with the earlier reports [38,39].

The room temperature PL spectra of the N:ZnO films show strong and sharp near bandedge UV emission at ~378 nm, as shown in Fig. 6. Besides the UV peak, a broad green emission band is observed from all the films. The green emission band can be deconvoluted into two Gaussian peaks. For the thin film grown on the Si substrate, the observed green emission bands are at 500 nm and 580 nm [Fig. 6(a)].

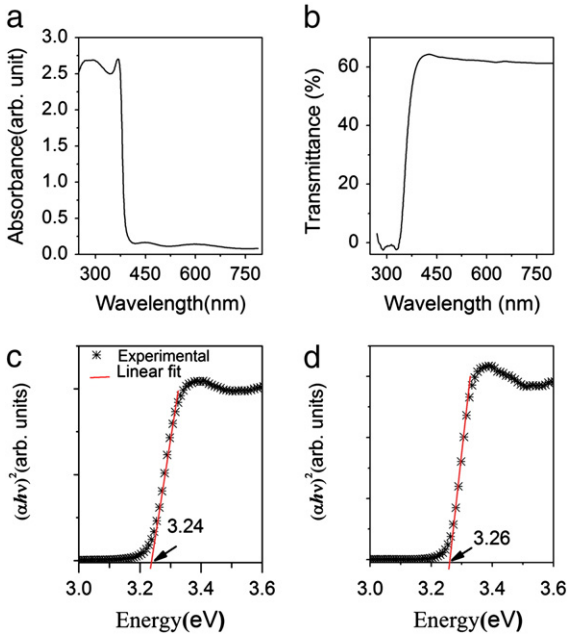


**Fig. 5.** (a) Optical absorption, and (b) transmittance spectra of as-deposited N:ZnO thin film grown on quartz substrate. (c) and (d) show the plot of $(\alpha h\nu)^2$ against the photon energy $h\nu$ to calculate the bandgap energy for the as-deposited and annealed N:ZnO film, respectively. Annealed thin film shows higher band gap.

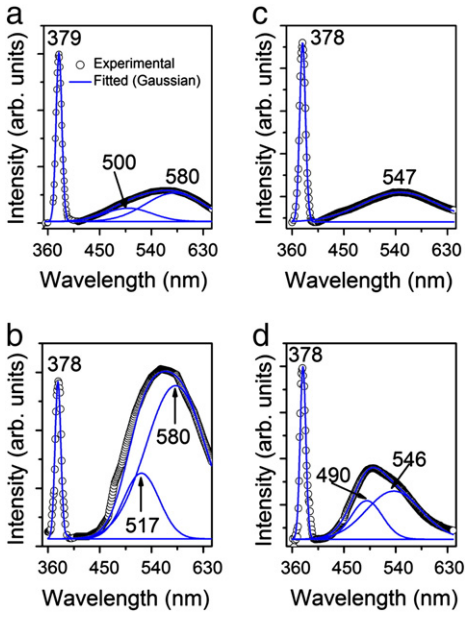


**Fig. 6.** Room temperature PL spectra of the as-deposited N:ZnO thin films grown on (a) Si and (b) alumina substrates. (c) and (d) show the PL spectra of corresponding annealed samples, respectively.

The preceding one is possibly due to emission from the oxygen vacancy states and later one corresponds to the intrinsic defect states in ZnO [40,41]. It has been suggested that zinc vacancies are also a possible source of the often observed green luminescence in ZnO [42]. As the sputtering was carried out without any additional flow of oxygen gas, possible formation of oxygen vacancy states on the surface of the N:ZnO films are expected. In contrast, zinc vacancies are deep acceptors and have high formation energies under *p*-type conditions [42]. Therefore, there is a strong possibility of formation of oxygen vacancy states in the N:ZnO thin films. Under the UV excitation, the oxygen vacancies result in green emission due to an excited-to-ground state transition [10,40]. Leiter et al.[43] have identified that oxygen vacancy as the defect responsible for the structure independent green emission band in ZnO, and demonstrated striking similarities of this defect to the anion vacancy in other ionic host crystals: BaO, SrO, CaO, and MgO. After the post-deposition annealing, the 500 nm and 580 nm components fully disappeared, which indicate that the oxygen vacancy and intrinsic defect states are significantly reduced after annealing. However, after annealing one new emission peak appears at 547 nm that corresponds to the presence of interstitial oxygen in ZnO [44]. During annealing the N:ZnO films are re-crystallized and oxygen vacancy are compensated by absorbing oxygen atoms from the air. The observed significant reduction in the 580 nm peak confirms the reduction of intrinsic defect states during re-crystallization. However absorption of more oxygen may cause formation of interstitial oxygen, which results a peak at 547 nm. In case of N:ZnO film on the alumina substrate, the intensity of the green emission band is higher than the UV emission band as shown in Fig. 6(b). After annealing, the intensity of the UV emission band is considerably enhanced, while the green emission band is correspondingly reduced. This implies that oxygen vacancies are still present in the annealed film and it may need longer time annealing to fully remove the associated defects. PL studies on as-deposited and annealed samples show that intrinsic defects are present in both cases and perhaps play a key role in the stability of the p-type conductivity of the N:ZnO. Though the exact mechanism of relatively stable p-type conduction in annealed N:ZnO films are not clear, it is likely that the defect complexes involving nitrogen impurity and oxygen/zinc interstitials may be responsible for the observed p-type behavior [24].

### 3.4. Photoconductivity studies

The PC of the N:ZnO film was measured by making contact on the surface of the film at a fixed distance of 3 mm between the two electrodes. A 200 μm thick aluminum wire was used for making electrical contact using silver paste with contact area ~0.25 $mm^2$. Since the N:ZnO film grown on Si substrate shows high electrical conductivity, it was chosen for PC studies. Fig. 7(a) shows the photocurrent-voltage characteristic of the annealed N:ZnO film grown on the Si substrate. The observed photocurrent increases linearly with the applied voltage indicating an Ohmic contact on the film. The photocurrent spectra [see Fig. 7(b)] measured at a bias voltage of 2 V show a sharp peak at 380 nm due to the band-edge absorption and generation of the photocarriers and two other peaks at 419 nm and 517 nm due to the photocarriers released from the two ingap defect states. For comparison, photocurrent spectrum of the undoped ZnO film measured with similar conditions is shown in Fig. 7(c), which shows similar features with three peaks located at 379, 418 and 494 nm. Note that the measured photocurrent in the annealed N:ZnO film is very high compared to the undoped film. This is likely to be caused by the large carrier concentration as measured from Hall effect and large grain size as seen from the SEM and AFM images of the N:ZnO film. A large surface area causes strong surface adsorption and higher PC. It is found that for excitation at 380 nm the PC of the N:ZnO film is enhanced by 335 times to that of the undoped ZnO film. This enhancement is very high compared to the earlier reports [21,25]. In a recent report, Liu et al. [45] shows the enhanced photoconduction from ZnO nanowires (NWs) by L-lysine passivation on the surface of the NWs. The L-lysine treatment suppressed the oxygen vacancy related states on the surface of the NWs and as a result an enhanced PC is observed. They also observed that NWs with fewer defects gain larger enhancement of PC. In our case, high carrier (hole) density, high mobility and presence of less defect states are believed to be responsible for the observed enhanced PC in the doped ZnO film. For the undoped ZnO film, the dark current is in the range of nA, but for the N:ZnO film it is of μA range. The high dark current in the N:ZnO film is the result of high carrier concentration and higher mobility. In our case, we observed a reduction in oxygen vacancy related defect states in the PL spectra after annealing the films. The reduction in defect density is partly responsible for the enhanced photoconduction, because very few photogenerated carriers can be trapped inside the defect states and most of the carriers can contributed to the photocurrent.

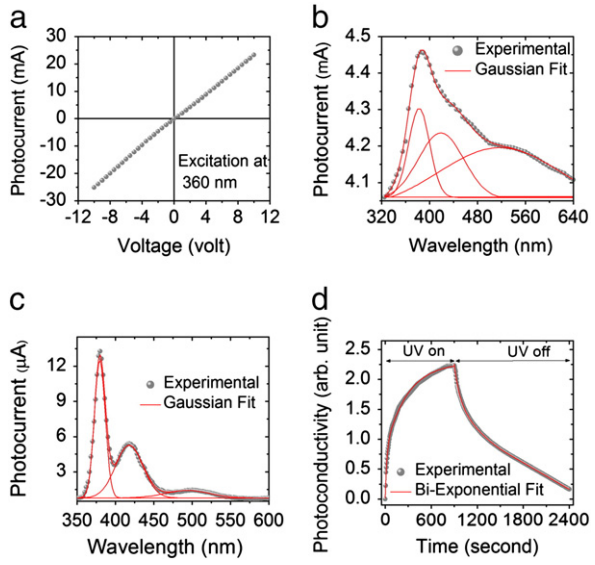


**Fig. 7.** (a) Photocurrent versus voltage at an excitation wavelength of 360 nm, (b) photocurrent as a function of wavelength for the annealed N:ZnO film on Si substrate, (c) Photocurrent spectra of the undoped ZnO film. (d) transient PC of the annealed N:ZnO thin film. The transient data fits to a bi-exponential growth and a bi-exponential decay. In each case, experimental data is shown with symbols and fitted data are shown with solid lines.

The transient PC was measured with the excitation wavelength of 360 nm at a bias voltage of 2 V and the result is shown in Fig. 7(d). The PC takes more than 10 min to reach the maximum value, indicating a slow photo-response of the doped film. On the other hand, undoped ZnO thin film show a relatively fast photoresponse, where PC reached the maximum within a few seconds. Tansley and Neely [46] also observed the similar slow photoresponse behavior as ours in vacuum. Ghosh et al. [47] reported high UV photoresponse from Cu doped as well as Cu–Li co-doped ZnO films. In the present case, the PC shows a bi-exponential growth and a bi-exponential decay behavior. The growth portion in the photoresponse curve is fitted with the equation,

$$\sigma(t) = A_1\left(1-e^{-t/\tau_1}\right) + A_2\left(1-e^{-t/\tau_2}\right) \quad (1)$$

where time constants are found to be $\tau_1 = 18$ s and $\tau_2 = 285$ s, indicating a very rapid photocurrent growth followed by a very slow growth process. The photoresponse of N:ZnO films consists of two parts: a rapid process of photogeneration and recombination of electron–hole pairs, and a slow process attributed to the surface adsorption and photodesorption of oxygen molecules due to the presence of defect states within the bandgap [25,48]. Similarly, when the UV light is turned off, the photocurrent show a rapid decay followed by a slow decay. The decay part can be fitted with a bi-exponential decay equation,

$$\sigma(t) = \sigma_0 + A_1 e^{-t/\tau_1} + A_2 e^{-t/\tau_2} \quad (2)$$

where the two relaxation time constants are calculated to be $\tau_1 = 67$ s and $\tau_2 = 680$ s, respectively. In the literature, similar bi-exponential decay behavior with time constants of several seconds has been reported for the undoped ZnO thin film [49]. When the UV light is off, i.e., during the decay process, the electron–hole recombination dominates, which corresponds to the faster decay component; so the conductivity decreases quickly at first. With the surface adsorption again, the conductivity comes to the initial value very slowly. During this process, chemisorbed oxygen species that act as a shallow trapping level establish equilibrium with the charge carriers, resulting in the slow photoresponse decay. Further, as revealed from the AFM and XRD studies, there exist nanocrystalline grains in the doped ZnO film and the carrier movement in such structures may be controlled by intercrystallite depletion barriers due to the presence of ionized adsorbates on nanocrystallite surfaces [46]. Surface rearrangement of mutually repulsive ions is expected to be a slow process that may give rise to such a slow photoresponse behavior as observed here.

## 4. Conclusions

In conclusion, we have achieved *p*-type conduction with improved stability and an enhanced PC in nitrogen doped *p*-type ZnO thin film grown by the RF sputtering method. The observed *p*-type conduction is retained even after 20 months for the annealed films, while the as-deposited films reverted back to n-type after a few days of growth. The stability of the annealed p-type films are discussed on the basis of morphology and structural improvement which possibly prevents the diffusion of impurities. We achieved a very low resistivity and a moderately high mobility p-type conduction in the N:ZnO film grown on Si substrate. Rectifying behavior of the *p*–*n* homo-junction formed on the doped ZnO film confirms the p-type conductivity of the N:ZnO layer. The suitability in the application of the grown p-type film is checked and found to be important for photodetection applications. A slow photoresponse with bi-exponential growth and decay behavior of the photocurrent is observed from the N:ZnO

film and it is ascribed to chemi-absorption of oxygen on the ZnO film exposed to air.

## References


[1] D.C. Look, D.C. Reynolds, J.R. Sizelove, R.L. Jones, C.W. Litton, G. Cantwell, W.C. Harsch, Solid State Commun. 105 (1998) 399.
[2] Z.K. Tang, G.K.L. Wong, P. Yu, M. Kawasaki, A. Ohtomo, H. Koinuma, Y. Segawa, Appl. Phys. Lett. 72 (1998) 3270.
[3] P. Nunes, E. Fortunato, P. Tonello, F.B. Fernandes, P. Vilarinho, R. Martins, Vacuum 64 (2002) 281.
[4] Y. Morinaga, K. Sakuragi, N. Fujimura, T. Ito, J. Cryst. Growth 174 (1997) 691.
[5] S.S. Shinde, P.S. Shinde, C.H. Bhosale, K.Y. Rajpure, J. Phys. D: Appl. Phys. 41 (2008) 105109.
[6] Z.H. Zhang, Z.Z. Ye, D.W. Ma, L.P. Zhu, T. Zhou, B.H. Zhao, Z.G. Fei, Mater. Lett. 59 (2005) 2732.
[7] B. Xiang, P. Wang, X. Zhang, S.A. Dayeh, D.P.R. Aplin, C. Soci, D. Yu, D. Wang, Nano Lett. 7 (2007) 323.
[8] G.D. Yuan, W.J. Zhang, J.S. Jie, X. Fan, J.X. Tang, I. Shafiq, Z.Z. Ye, C.S. Lee, S.T. Lee, Adv. Mater. 20 (2008) 168.
[9] J. Jie, G. Wang, X. Han, J.G. Hou, J. Phys. Chem. B 108 (2004) 17027.
[10] M.D. McCluskey, S.J. Jokela, J. Appl. Phys. 106 (2009) 071101.
[11] C. Zhang, X. Li, J. Bian, W. Yu, X. Gao, Solid State Commun. 132 (2004) 75.
[12] H. Matsui, H. Saeki, T. Kawai, H. Tabata, B. Mizobuchi, J. Appl. Phys. 95 (2004) 5882.
[13] D.C. Look, D.C. Reynolds, C.W. Litton, R.L. Jones, D.B. Eason, G. Cantwell, Appl. Phys. Lett. 81 (2002) 1830.
[14] A.V. Singh, R.M. Mehra, A. Wakahara, A. Yoshida, J. Appl. Phys. 93 (2003) 396.
[15] K.K. Kim, H.S. Kim, D.K. Hwang, J.H. Lim, S.J. Park, Appl. Phys. Lett. 83 (2003) 63.
[16] J.G. Lu, Z.Z. Ye, F. Zhuge, Y.J. Zeng, B.H. Zhao, L.P. Zhu, Appl. Phys. Lett. 85 (2004) 3134.
[17] C. Lee, S.Y. Park, J. Lim, H.W. Kim, Mater. Lett. 61 (2007) 2495.
[18] V. Vaithianathan, B.T. Lee, S.S. Kim, Appl. Phys. Lett. 86 (2005) 062101.
[19] T.M. Barnes, K. Olson, C.A. Wolden, Appl. Phys. Lett. 86 (2005) 112112.
[20] B. Yao, L.X. Guan, G.Z. Xing, Z.Z. Zhang, B.H. Li, Z.P. Wei, X.H. Wang, C.X. Cong, Y.P. Xie, Y.M. Lu, D.Z. Shen, J. Lumin. 122–123 (2007) 191.
[21] H.L. Porter, A.L. Cai, J.F. Muth, J. Narayan, Appl. Phys. Lett. 86 (2005) 211918.
[22] J.L. Lyons, A. Janotti, C.G. VandeWalle, Appl. Phys. Lett. 95 (2009) 252105.
[23] X.M. Duan, C. Stampfl, M.M.M. Bilek, D.R. McKenzie, Su-Huai Wei, Phys. Rev. B 83 (2011) 085202-1-8.
[24] Ren-Yu Tian, Yu-Jun Zhao, J. Appl. Phys. 106 (2009) 043707-1-6.
[25] Y.J. Zeng, Z.Z. Ye, Y.F. Lu, J.G. Lu, W.Z. Xu, L.P. Zhu, B.H. Zhao, Y. Che, Chem. Phys. Lett. 441 (2007) 115.
[26] S. Limpijumnong, L. Gordon, M.S. Miao, A. Janotti, C.G. VandeWalle, Appl. Phys. Lett. 97 (2010) 072112.
[27] X. Li, S.E. Asher, S. Limpijumnong, B.K. Keyes, C.L. Perkins, T.M. Barnes, H.R. Moutinho, J.M. Luther, S.B. Zhang, S.H. Wei, T.J. Coutts, J. Cryst. Growth 287 (2006) 94.
[28] B.D. Cullity, S.R. Stock, Elements of X-Ray Diffraction, 3rd ed. Prentic Hall, NJ, 2001.
[29] R. Keezer, J. Appl. Phys. 35 (1961) 1866.
[30] A. Kaschner, U. Haboeck, Martin Strassburg, Matthias Strassburg, G. Kaczmarczyk, A. Hoffmann, C. Thomsen, Appl. Phys. Lett. 80 (2002) 1909.
[31] D.C. Look, Semicond. Sci. Technol. 20 (2005) S55.
[32] O. Bierwagen, T. Ive, C.G. VandeWalle, Appl. Phys. Lett. 93 (2008) 242108-1-3.
[33] J. Wang, V. Sallet, F. Jomard, A.M.B. doRego, E. Elamurugu, R. Martins, E. Fortunato, Thin Solid Films 515 (2007) 8780.
[34] A. Tsukazaki, A. Ohtomo, T. Onuma, M. Ohtani, T. Makino, M. Sumiya, K. Ohtani, S.F. Chichibu, S. Fuke, Y. Segawa, H. Ohno, H. Koinuma, M. Kawasaki, Nat. Mater. 4 (2005) 42.
[35] T. Ohgaki, N. Ohashi, S. Sugimura, H. Ryoken, I. Sakaguchi, Y. Adachi, H. Haneda, J. Mater. Res. 23 (2008) 2293.
[36] D.K. Schroder, Semiconductor Material and Device Characterization, 3rd ed., Wiley-Interscience, New Jersey, USA, 2006, p. 38.
[37] M. Pan, R. Rondon, J. Cloud, V. Rengarajan, W. Nemeth, A. Valencia, J. Gomez, N. Spencer, J. Nause, Proc. SPIE 6122 (2006) 61220M.
[38] A. Thean, J.P. Leburton, Appl. Phys. Lett. 79 (2001) 1030.
[39] X. Yang, A. Wolcott, G. Wang, A. Sobo, R.C. Fitzmorris, F. Qian, J.Z. Zhang, Y. Li, Nano Lett. 9 (2009) 2331.
[40] K. Vanheusden, W.L. Warren, C.H. Seager, D.K. Tallant, J.A. Voigt, B.E. Gnade, J. Appl. Phys. 79 (1996) 7983.
[41] P.K. Giri, S. Bhattacharyya, D.K. Singh, R. Kesavamoorthy, B.K. Panigrahi, K.G.M. Nair, J. Appl. Phys. 102 (2007) 093515.
[42] A. Janotti, C.G.V.d. Walle, Phys. Rev. B 76 (2007) 165202.
[43] F.H. Leiter, H.R. Alves, A. Hofstaetter, D.M. Hoffmann, B.K. Meyer, Phys. Status Solidi B 226 (2001) R4.
[44] B. Lin, Z. Fu, Y. Jia, Appl. Phys. Lett. 79 (2001) 943.
[45] J. Liu, J. Park, K.H. Park, Y. Ahn, J. Park, K.H. Koh, S. Lee, Nanotechnol 21 (2010) 485504.
[46] T.L. Tansley, D.F. Neely, Thin Solid Films 121 (1984) 95.
[47] T. Ghosh, D. Basak, J. Phys. D: Appl. Phys. 42 (2009) 145304.
[48] Q.H. Li, T. Gao, T.H. Wang, Appl. Phys. Lett. 86 (2005) 123117-1-3.
[49] S. Mridha, D. Basak, Appl. Phys. Lett. 92 (2008) 142111-1-3.